

Metal–Organic Frameworks

A Metal–Organic Framework Containing Unusual Eight-Connected Zr–Oxo Secondary Building Units and Orthogonal Carboxylic Acids for Ultra-sensitive Metal Detection

Michaël Carboni, Zekai Lin, Carter W. Abney, Teng Zhang, and Wenbin Lin^{*[a]}

Abstract: Two metal–organic frameworks (MOFs) with Zr–oxo secondary building units (SBUs) were prepared by using *p,p'*-terphenyldicarboxylate (TPDC) bridging ligands pre-functionalized with orthogonal succinic acid (MOF-1) and maleic acid groups (MOF-2). Single-crystal X-ray structure analysis of MOF-1 provides the first direct evidence for eight-connected SBUs in UiO-type MOFs. In contrast, MOF-2 contains twelve-connected SBUs as seen in the traditional UiO MOF topology. These structural assignments were confirmed by extended X-ray absorption fine structure (EXAFS) analysis. The highly porous MOF-1 is an excellent fluorescence sensor for metal ions with the detection limit of <0.5 ppb for Mn²⁺ and three to four orders of magnitude greater sensitivity for metal ions than previously reported luminescent MOFs.

Metal–organic frameworks (MOFs) are a class of hybrid materials built from metal ions or clusters bridged by organic linkers.^[1] Due to their high porosity, stability, and tunability, these materials are attractive for diverse applications.^[2] Decorating the bridging ligand with an orthogonal functionality represents an effective strategy to functionalize MOF channels for potential applications. The incorporation of amine, carboxylic acid, and other functional groups into MOFs has indeed resulted in promising materials for CO₂ sorption,^[3] chemical sensing^[4] and catalysis.^[2e,5] Direct synthesis of MOFs using pre-functionalized ligands is challenging, as the orthogonal moieties may coordinate metals during MOF preparation. While postsynthetic modification (PSM)^[6] and protection/deprotection^[7] are effective strategies for introducing these functionalities, quantitative functionalization is rarely achieved. As a result, few examples of MOFs containing non-coordinated orthogonal functionalities have been reported, either through use of pre-functionalized ligands^[8] or via PSM processes,^[9] severely limiting the applications of many MOFs.

First reported by Lillerud and co-workers, the UiO family of MOFs possess a robust Zr₆O₄(OH)₄(RCO₂)₁₂ secondary building unit (SBU) and are stable under a wide range of conditions.^[10] Using a *p,p'*-terphenyldicarboxylic (TPDC) ligand pre-functionalized with a phosphorylurea moiety, we recently demonstrated this UiO platform was sufficiently stable for extracting U^{VI} from aqueous solutions.^[11] While the high connectivity of the Zr₆O₄(OH)₄(RCO₂)₁₂ SBU helps to stabilize the MOF structure, partial removal of ligands would result in a larger pore aperture, enhancing the rate of diffusion into the MOF interior and permitting larger molecules to be internalized. Recent publications reveal the addition of acid modulators during synthesis results in UiO materials with increased surface area and larger pore sizes.^[12] It has been proposed that these effects are due to formation of site defects at the MOF SBUs, resulting in fewer than twelve dicarboxylate bridging ligands connecting the Zr–oxo clusters. This postulation was supported through various indirect analyses, such as thermogravimetric analysis (TGA), ¹⁹F NMR, and IR spectroscopy,^[13] as well as more advanced techniques such as PXRD/EXAFS^[14] and high-resolution neutron power diffraction,^[15] but has thus far evaded single-crystal X-ray diffraction analysis owing to the randomly distributed and stochastically oriented site defects in the previous UiO MOF materials.

Herein, we report the preparation of two MOFs based on Zr–oxo SBUs and TPDC ligands pre-functionalized with orthogonal moieties terminating with succinic acid (MOF-1) and maleic acid (MOF-2). Single-crystal X-ray structure analyses revealed eight-connected Zr₆O₈(OH)₈(RCO₂)₈ SBUs in MOF-1 and twelve-connected Zr₆O₄(OH)₄(RCO₂)₁₂ SBUs in MOF-2, which was confirmed by fitting EXAFS data. MOF-1 provides the first direct evidence for a UiO-type MOF possessing a SBU with fewer than twelve bridging ligands. MOF-1 exhibits larger pore apertures than MOF-2 and is highly sensitive for detecting metal ions via fluorescence quenching.

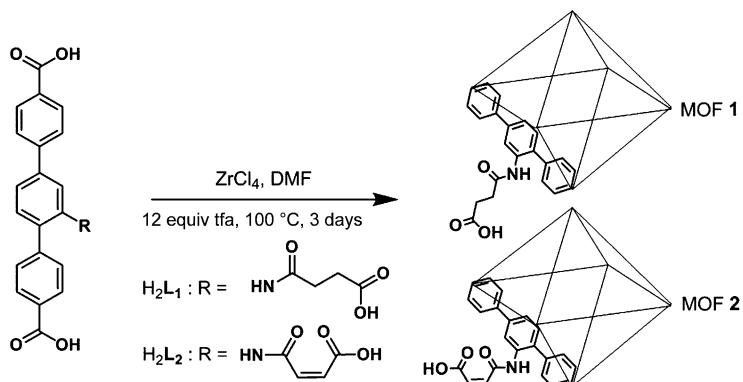
The TPDC ligands with orthogonal succinic acid and maleic acid functionalities, H₂L₁ and H₂L₂, were prepared by treating 2,5-bis(4-carboxyphenyl)aniline (TPDC-NH₂) with succinic or maleic anhydride in dry DMSO at room temperature for 12 h. Following solvent removal, the solid was washed with water and ethanol, then dried under vacuum to afford pure H₂L₁ and H₂L₂ ligands. Crystals of MOF-1 and MOF-2 were obtained by heating a solution of ZrCl₄, H₂L₁ or H₂L₂, and trifluoroacetic acid (TFA) in DMF at 100 °C for three days (Scheme 1).

A single-crystal X-ray diffraction study showed that MOF-1 crystallizes in the tetragonal *I*4/*mmm* space group (Figure 1).

[a] Dr. M. Carboni,[†] Z. Lin,[†] C. W. Abney, T. Zhang, Prof. Dr. W. Lin
Department of Chemistry
University of Chicago
929 E 57th Street, Chicago, IL 60637 (USA)
E-mail: wenbinlin@uchicago.edu

[†] These authors contributed equally to this work.

Supporting information for this article is available on the WWW under
<http://dx.doi.org/10.1002/chem.201405194>.



Scheme 1. Direct synthesis of MOFs **1** and **2** with pre-functionalized ligands possessing orthogonal carboxylic acid moieties.

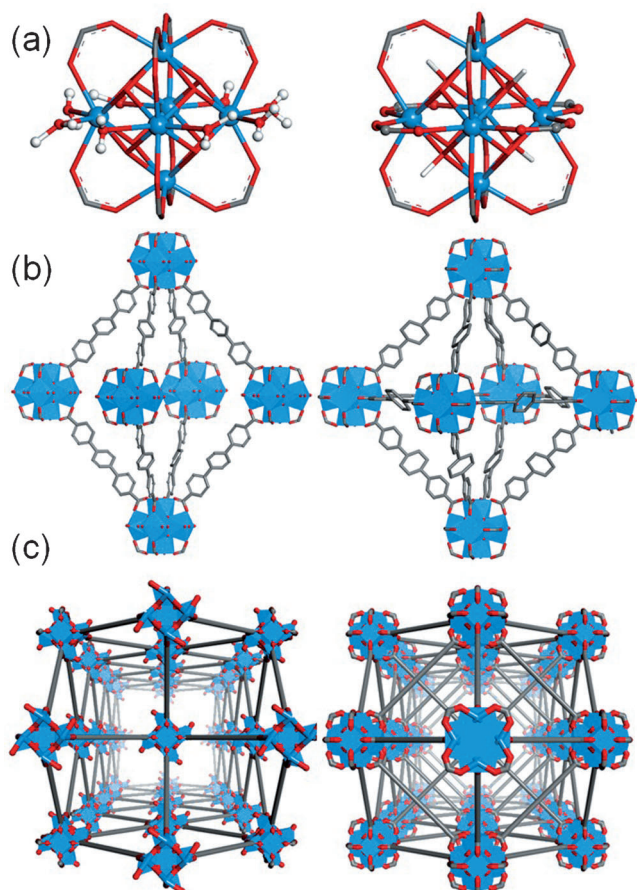


Figure 1. Comparison of eight- and twelve-connected MOF topologies from the UiO family. The figures for eight-connected MOF-1 are displayed on the left, and the figures for twelve-connected MOF-2 are shown on the right. a) SBUs, b) octahedral cavities, and c) perspective views along the z axis. Channels of both MOFs show distinct differences as a result of different SBU connectivity. Blue polyhedra and spheres are Zr atoms, with red and grey representing oxygen and carbon, respectively. Hydrogen atoms are omitted for clarity, with the exception of those on equatorial water molecules and bridging $\mu_3\text{-OH}$ groups on the SBUs.

The asymmetric unit consists of 1/16 of the $\text{Zr}_6\text{O}_8(\text{OH}_2)_8(\text{CO}_2)_8$ -cluster and 1/4 of the bridging ligands. Unlike traditional UiO MOFs, the Zr SBU in MOF-1 is only eight-connected, with the

formula of $\text{Zr}_6\text{O}_8(\text{OH}_2)_8(\text{L}_1)_4$. Compared to a typical $\text{Zr}_6\text{O}_8(\text{OH})_4(\text{L})_6$ cluster, the four bridging carboxylate groups on the equatorial plane of the Zr_6 octahedra are missing, substituted by aqua coordination. The resulting MOF possesses **bcu** network topology with $\{4^{24}\cdot6^4\}$ connectivity. Although a similar SBU has been reported in Zr MOFs constructed from tetracarboxylate ligands,^[16] this is the first direct crystallographic evidence for an eight-connected Zr SBU with a linear bridging ligand, confirming the earlier proposal put forward by Lillerud, Zhou, De Vos, and Hupp.^[12-14]

MOF-2 crystallizes in the cubic $Fm\bar{3}m$ space group. The asymmetric unit consists of 1/48 of the $\text{Zr}_6\text{O}_8(\text{OH})_4(\text{CO}_2)_{12}$ cluster and 1/8 of the bridging ligands. The SBU comprises six Zr cations, with each Zr bridged by $\mu_3\text{-O}$, $\mu_3\text{-OH}$, and carboxylate groups. Each SBU is connected to twelve neighboring SBUs by twelve dicarboxylate linkers. Like other well-established UiO MOFs, MOF-2 possesses **fcu** network topology.

Owing to the crystallographically imposed disorder for the bridging ligands in UiO-type MOFs, the identities of the bridging ligands in MOFs **1** and **2** cannot be established by single-crystal X-ray structure analyses. Instead, the identities of bridging ligands in MOFs **1** and **2** were determined by integration of proton peaks in the ^1H NMR spectra of digested samples of MOFs **1** and **2** (in $\text{K}_3\text{PO}_4/\text{D}_2\text{O}/[\text{D}_6]\text{DMSO}$). ^1H NMR spectroscopy unambiguously revealed that the H_2L_1 ligand did not decompose during the MOF synthesis; the ^1H NMR spectrum obtained for digested MOF-1 (Figure S7c) matches perfectly with that of pure ligand H_2L_1 in a solution of $\text{K}_3\text{PO}_4/\text{D}_2\text{O}/[\text{D}_6]\text{DMSO}$ (Figure S7b). ESI-MS analysis (Figure S8) confirms the purity of the digested MOF-1 with a unique peak at m/z 432.1 corresponding to $[\text{H}_2\text{L}_1\text{-H}]^-$. Unlike MOF-1, significant decomposition of the ligand is observed in the ^1H NMR spectrum of digested MOF-2 (Figure S9). Integration of the ethylene peaks ($\delta=5.75$ and 6.25 ppm) indicate that approximately 25% of the original L_2 ligand remained intact after MOF synthesis. This was further supported by ESI-MS analysis (Figure S10) exhibiting signals at m/z 432.1 ($[\text{H}_2\text{L}_2+\text{H}]^+$), m/z 470.1 ($[\text{H}_2\text{L}_2+\text{K}]^+$), and m/z 334.1 ($[\text{TPDC-NH}_2+\text{H}]^+$). The decomposition of H_2L_2 can be reduced to 50% by decreasing the duration of MOF-2 synthesis to one day, while prolonged heating (7 days) results in 91% degradation of L_2 ligands (Figure S11). The difference in topology can be attributed to the hydrolysis of the orthogonal functionality in MOF-2, alleviating steric effects and accommodating formation of a twelve-connected SBU.

TGA results were consistent with the formulations of MOFs **1** and **2** as established by X-ray crystallography and NMR analyses (Table S1). While the TGA profile obtained for MOF-1 is in agreement with the presence of pure L_1 ligands, the TGA data for MOF-2 are consistent with partial decomposition of L_2 ligands during MOF synthesis.

In spite of the significant structural difference between MOFs **1** and **2**, their PXRD patterns appear remarkably similar (Figure 2c), thus offering no insight into the number of bridging ligands linking the SBUs in the bulk materials of MOFs **1** and **2**. We have utilized X-ray absorption spectroscopy (XAS)

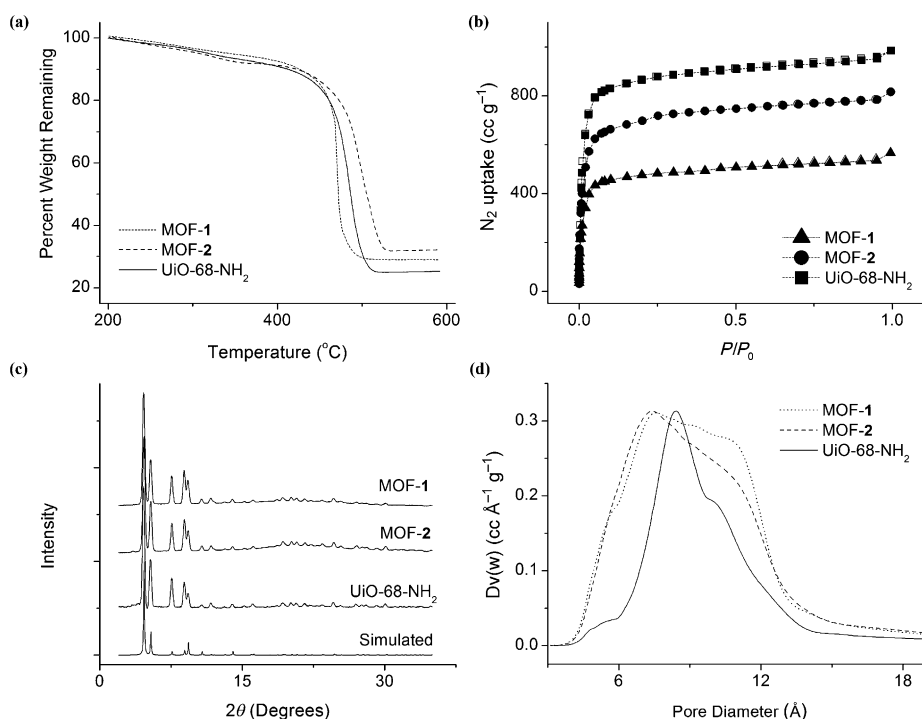


Figure 2. a) TGA curves, b) N_2 uptake isotherms, c) powder X-ray patterns, and d) pore size distributions for $UiO-68-NH_2$, MOF-1, and MOF-2.

to lend additional support for the structural assignments of MOFs **1** and **2** and to prove the phase purity of these functionalized UiO materials. MOF-1, MOF-2, and $UiO-68-NH_2$ were investigated by XAS at the Zr K-edge, with data processed and analyzed by using the Athena and Artemis programs of the IFEFFIT package based on FEFF 6.^[17] A comparison of the X-ray absorption near-edge (XANES) region reveals slight differences between the three MOFs (Figure S22 and S23). MOF-1 has slightly lower intensity in the XANES region when compared to MOF-2 and $UiO-68-NH_2$. As XAS measures the average spectrum for all absorbing elements, this difference in pre-edge intensity can be attributed to the presence of two crystallographically inequivalent Zr centers in the SBUs: the axial Zr centers are coordinated by four μ_3 -oxo groups and four carboxylic oxygen, whereas the equatorial Zr centers are coordinated by four μ_3 -oxo groups, two carboxylic oxygen, and two coordinating water molecules. For MOF-2 and $UiO-68-NH_2$, all Zr are crystallographically equivalent, and their XANES spectra are identical in intensity.

Fits for the extended (EXAFS) region for all three MOFs were also performed, using the corresponding crystal structures as models. Fits yielded only minor changes in half path length, reasonable values for Debye–Waller parameters, and final R -factors less than 0.02 in all instances, indicating <2% misfit. The fits of MOF-1 with an eight-connected model and MOF-2 with a twelve-connected model are shown in Figure 3, while the fit of $UiO-68-NH_2$ and fitting parameters are available in the Supporting Information.

Analysis of the EXAFS fits reveals some differences between the Zr coordination environments in MOF-1, MOF-2, and $UiO-$

$68-NH_2$, as is expected from the different SBUs obtained by single-crystal diffraction (Figure 3). The spectral component attributable to single scattering off the bridging μ_3 -oxo group indicates a shorter path length for MOF-1 than the other two MOFs. This is expected, as the twelve-connected UiO is known to have alternating μ_3 -oxo/ μ_3 -hydroxo species to accommodate charge balance in the SBU, while the eight-connected SBU would only possess μ_3 -oxo moieties. The single scattering path off of the carboxylic carbon is longer for MOF-2 than MOF-1 or $UiO-68$. A minimal signal is observed in this region due to destructive interference from multiple scattering paths,^[14] making definitive analysis challenging. Importantly, the inclusion of a $Zr-OH_2$ scattering path was essential to obtain a good fit for MOF-1, as the $Zr-O$ bond

lengths for the μ_3 -oxo and carboxylic oxygen are 0.25 and 0.1 Å shorter, respectively. The high quality of these EXAFS fits confirm the phase purity and structure of the MOFs as determined by single-crystal analysis.

Permanent porosity of MOFs **1** and **2** were determined after removal of solvent molecules by a previously published freeze-drying process.^[18] Nitrogen sorption at 77 K showed type I isotherms for both MOFs **1** and **2** as well as $UiO-68-NH_2$, indicative of their microporous structures. The BET surface areas for MOFs **1** and **2** were slightly lower than that of $UiO-68-NH_2$ due to functionalization of the bridging ligand (2101, 3025, and 3750 $m^2 g^{-1}$ for MOF-1, MOF-2, and $UiO-68-NH_2$, respectively). The much lower surface area of MOF-1 suggests significant framework distortion in the solvent-free MOF; such framework breathing phenomena have been observed for many MOFs with large open channels.^[2e, 19] The reduced surface area of MOF-1 is thus consistent with the structural differences between the three MOFs, as the eightfold connectivity at the SBU of MOF-1 is more susceptible to framework breathing even following solvent removal under mild conditions. The pore size distribution of MOF **1** and **2** was broader than that of $UiO-68-NH_2$, with pore apertures spanning 7–12 Å.

The orthogonal amide and carboxylic acid groups within the MOF channel are expected to have high affinity for transition metal cations. As MOF-1 displays a broad emission band at 390 nm upon excitation at 330 nm, chelating of transition metal cations will likely lead to changes of the fluorescence intensity. MOFs have been investigated for various sensing applications, often taking advantage of the intrinsic fluorescence of the aromatic bridging ligands or luminescence of the metals in

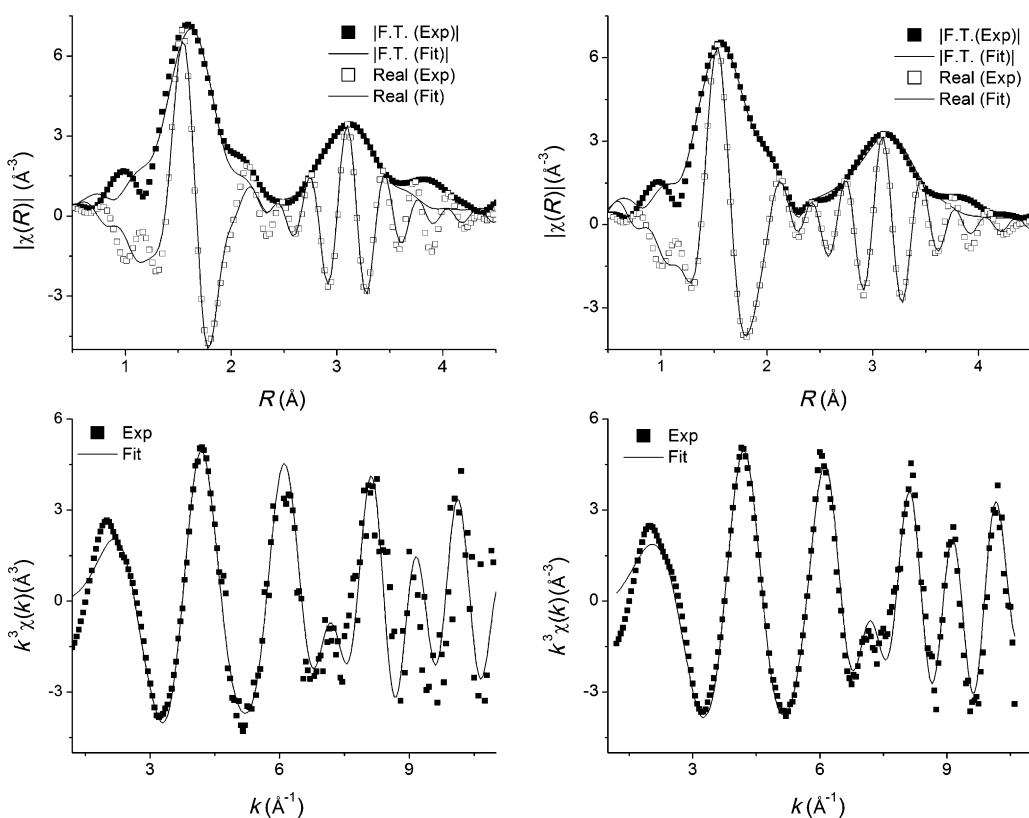


Figure 3. Comparison between experimental EXAFS data (squares) and best fits (line) for MOF-1 (left) and MOF-2 (right). Top panels are displayed in R -space containing both magnitude of Fourier Transform and real components. Bottom panels display k^3 -weighted $\chi(k)$ data and fits. Final R -factors of 0.02 and < 0.01 were obtained for MOFs 1 and 2, respectively.

the SBU.^[4c,20] MOFs have also been applied to metal sensing specifically, with emphasis on detection of Cu^{2+} , Fe^{3+} , Ag^+ , Tb^{3+} , and Eu^{3+} .^[4a,21] Despite extensive research, the best metal-sensing MOFs in the literature possess detection limits of 20 ppb^[21e] and K_{sv} values of 250 mM^{-1} .^[21c] We performed fluorescence quenching studies of MOF-1 with different metal cations ($M^{2+} = \text{Fe}^{2+}$, Mn^{2+} , Co^{2+} , Cd^{2+} , Cu^{2+} , Ni^{2+} , Zn^{2+} , and Mg^{2+}) in MeOH solutions. The fluorescence signals of MOF 1 were measured in the presence of various metal ions in different concentrations (Figure 4) and the Stern–Völmer constants are summarized in Table 1.

As shown in Table 1, transition metal ions with unpaired d-electrons such as Mn^{2+} , Cu^{2+} , Fe^{2+} , Co^{2+} , and Ni^{2+} exhibited

Table 1. Stern–Völmer constants of MOF 1 and homogeneous controls with different metal quenchers.

| Metal ions | $K_{\text{SV}} [\text{mM}^{-1}]$ (MOF-1) | $K_{\text{SV}} [\text{mM}^{-1}]$ (Me_2L_1) | Preconcentration factor |
|------------------|---|---|-------------------------|
| Fe^{2+} | 264.2 ± 7.6 | 4.7 ± 0.7 | 202 |
| Mn^{2+} | 906.5 ± 41.2 | -11.3 ± 3.12 | 300 |
| Co^{2+} | 207.8 ± 6.2 | 10.5 ± 2.7 | 76 |
| Cd^{2+} | 2.2 ± 0.1 | -1.2 ± 0.1 | – |
| Cu^{2+} | 468.0 ± 19.9 | -1.3 ± 6 | 501 |
| Ni^{2+} | 134.0 ± 6.2 | 38.8 ± 1.9 | 173 |
| Zn^{2+} | 21.7 ± 1.4 | -29.4 ± 2.1 | 120 |
| Mg^{2+} | 1.0 ± 0.1 | -1.9 ± 0.2 | 50 |

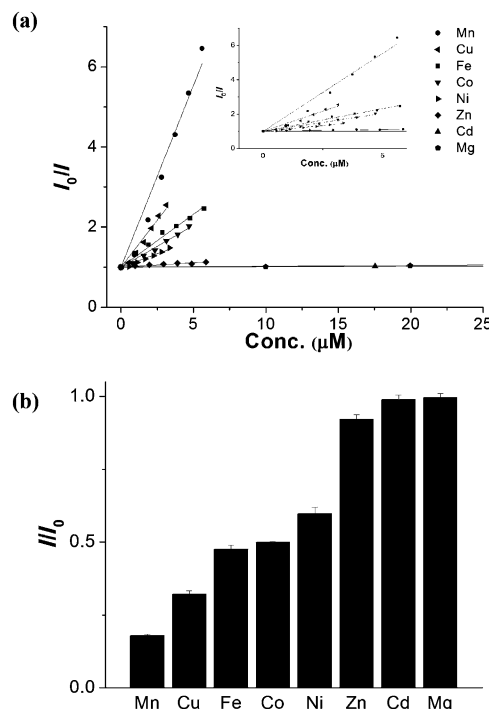


Figure 4. a) Stern–Völmer (SV) plots of the fluorescence emissions of MOF 1 quenched by different metals in MeOH with 330 nm excitation (emission decays were monitored at 390 nm). Inset: Magnification of SV plots in the low concentration range. b) Fluorescence intensity of MOF-1 in 4.5 μM MeOH solutions of different metals.

significant quenching effects, while diamagnetic cations such as Mg^{2+} , Zn^{2+} , and Cd^{2+} had negligible effects upon fluorescence. The proposed quenching mechanism is enhanced non-radiative deactivation in the presence of nearby unpaired spins. The fluorescence quenching follows the Stern–Völmer (SV) equation: $I_0/I = 1 + K_{SV}[M]$, where I_0 and I correspond to the luminescence intensity for MOF-1 in absence and presence of metal cations, respectively, $[M]$ is the metal concentration, and K_{SV} is the Stern–Völmer constant. MOF-1 shows dramatic fluorescence quenching at very low metal concentrations, with remarkable sensitivity to Mn^{2+} and Cu^{2+} over other metal ions. An exceptionally high K_{SV} value of $(0.91 \pm 0.04) \times 10^6 \text{ M}^{-1}$ was obtained for Mn^{2+} , while K_{SV} for Cu^{2+} was $(0.47 \pm 0.02) \times 10^6 \text{ M}^{-1}$ (Table 1). The sensitivity of MOF-1 is three to four orders of magnitude higher than that for previously reported MOFs with K_{SV} values in the range of tens to hundreds M^{-1} .^[4a, 21b] Quenching studies were also conducted on the homogeneous compound Me_2L_1 under identical experimental conditions, however, no fluorescence quenching was observed for any of the metal cations except Ni^{2+} , which exhibits modest quenching of the Me_2L_1 fluorescence (Figure S13–S20). Furthermore, investigation of MOF-1 by PXRD after soaking in 45 mM Mn^{2+} solution overnight reveals no loss of crystallinity (Figure S21).

The enhancement of fluorescent quenching at low concentrations can be partly attributed to preconcentration of metal ions within the MOF channels. To verify this, we soaked MOF-1 in solutions of different metal cations (50 μM) and determined the distribution of metal cations in the supernatant and MOF channels by inductively coupled plasma mass spectrometry (ICP-MS). ICP-MS analysis indicated that the concentrations of 12.2 mM of Mn^{2+} and 7.6 mM of Cu^{2+} within the channels of MOF-1 respectively, which were 300 and 501 times more concentrated than that in the supernatant (Table 1).

To further corroborate the high sensitivity of MOF-1 compared to other reported systems, we determined the detection limit for Mn^{2+} first by the Taylor method,^[22] then confirmed experimentally. The absolute standard deviations of the calibrators were plotted against their respective concentrations to give the background level S_0 as the y-intercept of the plot. The detection limit was estimated to be $3S_0$, which equals 0.6 ppb. Experimentally, the fluorescence intensity of the MOF solutions was determined to be 347.10 ± 3.94 and decreased to 321.71 ± 4.32 with the addition of 0.5 ppb Mn^{2+} . The experiment indicated that the detection limit for Mn^{2+} was below 0.5 ppb, consistent with the estimation by the Taylor method.

In summary, we have successfully prepared two Zr MOFs by pre-functionalization of the TPDC-NH₂ ligand with succinic acid and maleic anhydride. Single-crystal analysis and EXAFS fits of MOF-1 provide the first direct evidence of a UiO type SBU possessing reduced connectivity, while MOF-2 possesses the traditional twelve-connected motif. Due to the highly accessible metal-binding sites located at the terminus of the orthogonal functionalities, MOF-1 serves as a highly sensitive fluorescent sensor for metal ions, capable of detecting Mn^{2+} at concentrations less than 0.5 ppb. MOF-1 was >1000 times more sensitive for metal cations than previously reported MOFs, demon-

strating the utility of orthogonal functionalities for developing highly sensitive MOF-based sensors.

Experimental Section

See Supporting Information for details. CCDC-1012331 (MOF-1), and CCDC-1012332 (MOF-2) contain the supplementary crystallographic data for this paper. These data can be obtained free of charge from The Cambridge Crystallographic Data Centre via www.ccdc.cam.ac.uk/data_request/cif.

Acknowledgements

This work was supported by the DoE Office of Nuclear Energy's Nuclear Energy University Program (Sub-Contract - 20 #120427, Project-#3151). XAS analysis was performed at GeoSoilEnviroCARS (Sector 13), Advanced Photon Source (APS), Argonne National Laboratory. GeoSoilEnviroCARS is supported by the National Science Foundation - Earth Sciences (EAR-1128799) and Department of Energy (DOE)- GeoSciences (DE-FG02-94ER14466). Single-crystal diffraction studies were performed at ChemMatCARS (Sector 15), APS, Argonne National Laboratory. ChemMatCARS is principally supported by the Divisions of Chemistry (CHE) and Materials Research (DMR), National Science Foundation, under grant number NSF/CHE-1346572. Use of the APS, an Office of Science User Facility operated for the U.S. DOE Office of Science by Argonne National Laboratory, was supported by the U.S. DOE under Contract No. DE-AC02-06CH11357. We thank the University of Chicago Physical Science Division Mass Spectrometry and NMR facilities for instrumentation.

Keywords: crystal structures • fluorescence sensing • functionalization • metal sensing • metal–organic frameworks

- [1] a) B. F. Hoskins, R. Robson, *J. Am. Chem. Soc.* **1989**, *111*, 5962–5964; b) M. Eddaoudi, J. Kim, N. Rosi, D. Vodak, J. Wachter, M. O'Keeffe, O. M. Yaghi, *Science* **2002**, *295*, 469–472; c) M. Eddaoudi, D. B. Moler, H. Li, B. Chen, T. M. Reineke, M. O'Keeffe, O. M. Yaghi, *Acc. Chem. Res.* **2001**, *34*, 319–330; d) S. Subramanian, M. J. Zaworotko, *J. Chem. Soc. Chem. Commun.* **1993**, 952–954; e) S. Kitagawa, S. Matsuyama, M. Munakata, T. Emori, *J. Chem. Soc. Dalton Trans.* **1991**, 2869–2874; f) S. Kitagawa, S. Matsuyama, M. Munakata, N. Osawa, H. Masuda, *J. Chem. Soc. Dalton Trans.* **1991**, 1717–1720; g) O. R. Evans, R.-G. Xiong, Z. Wang, G. K. Wong, W. Lin, *Angew. Chem. Int. Ed.* **1999**, *38*, 536–538; *Angew. Chem.* **1999**, *111*, 557–559; h) G. Férey, C. Mellot-Draznieks, C. Serre, F. Millange, *Acc. Chem. Res.* **2005**, *38*, 217–225.
- [2] a) M. D. Allendorf, C. A. Bauer, R. K. Bhakta, R. J. T. Houk, *Chem. Soc. Rev.* **2009**, *38*, 1330–1352; b) G. Férey, *Chem. Soc. Rev.* **2008**, *37*, 191–214; c) C. Wang, D. Liu, W. Lin, *J. Am. Chem. Soc.* **2013**, *135*, 13222–13234; d) L. Ma, C. Abney, W. Lin, *Chem. Soc. Rev.* **2009**, *38*, 1248–1256; e) P. Horcajada, T. Chalati, C. Serre, B. Gillet, C. Sebrie, T. Baati, J. F. Eubank, D. Heurtault, P. Clayette, C. Kreuz, J.-S. Chang, Y. K. Hwang, V. Marsaud, P.-N. Bories, L. Cynober, S. Gil, G. Férey, P. Couvreur, R. Gref, *Nat. Mater.* **2010**, *9*, 172–178; f) J. S. Seo, D. Whang, H. Lee, S. I. Jun, J. Oh, Y. J. Jeon, K. Kim, *Nature* **2000**, *404*, 982–986; g) C. K. Brozek, M. Dincă, J. Am. Chem. Soc. **2013**, *135*, 12886–12891; h) N. Yanai, K. Kitayama, Y. Hijikata, H. Sato, R. Matsuda, Y. Kubota, M. Takata, M. Mizuno, T. Uemura, S. Kitagawa, *Nat. Mater.* **2011**, *10*, 787–793; i) Z. R. Herm, B. M. Wiers, J. A. Mason, J. M. van Baten, M. R. Hudson, P. Zajdel, C. M. Brown, N. Masciocchi, R. Krishna, J. R. Long, *Science* **2013**, *340*, 960–964.

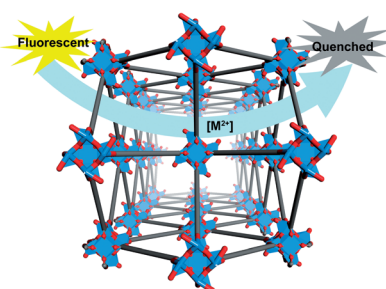
- [3] a) F. Luo, M. S. Wang, M. B. Luo, G. M. Sun, Y. M. Song, P. X. Li, G. C. Guo, *Chem. Commun.* **2012**, *48*, 5989–5991; b) N. Reimer, B. Gil, B. Marszalek, N. Stock, *Crystengcomm* **2012**, *14*, 4119–4125; c) A. Torrisi, R. G. Bell, C. Mellot-Draznieks, *Cryst. Growth Des.* **2010**, *10*, 2839–2841; d) A. M. Fracaroli, H. Furukawa, M. Suzuki, M. Dodd, S. Okajima, F. Gándara, J. A. Reimer, O. M. Yaghi, *J. Am. Chem. Soc.* **2014**, *136*, 8863–8866; e) T. M. McDonald, W. R. Lee, J. A. Mason, B. M. Wiers, C. S. Hong, J. R. Long, *J. Am. Chem. Soc.* **2012**, *134*, 7056–7065.
- [4] a) B. L. Chen, L. B. Wang, Y. Q. Xiao, F. R. Fronczeck, M. Xue, Y. J. Cui, G. D. Qian, *Angew. Chem. Int. Ed.* **2009**, *48*, 500–503; *Angew. Chem.* **2009**, *121*, 508–511; b) M. M. Wanderley, C. Wang, C. D. Wu, W. B. Lin, *J. Am. Chem. Soc.* **2012**, *134*, 9050–9053; c) Z. Xie, L. Ma, K. E. deKrafft, A. Jin, W. Lin, *J. Am. Chem. Soc.* **2009**, *131*, 922–923; d) R.-B. Lin, F. Li, S.-Y. Liu, X.-L. Qi, J.-P. Zhang, X.-M. Chen, *Angew. Chem. Int. Ed.* **2013**, *52*, 13429–13433; *Angew. Chem.* **2013**, *125*, 13671–13675.
- [5] a) K. Manna, T. Zhang, W. Lin, *J. Am. Chem. Soc.* **2014**, *136*, 6566–6569; b) J. M. Falkowski, T. Sawano, T. Zhang, G. Tsun, Y. Chen, J. V. Lockard, W. Lin, *J. Am. Chem. Soc.* **2014**, *136*, 5213–5216; c) M. B. Lalonde, O. K. Farha, K. A. Scheidt, J. T. Hupp, *ACS Catal.* **2012**, *2*, 1550–1554; d) K. Mo, Y. Yang, Y. Cui, *J. Am. Chem. Soc.* **2014**, *136*, 1746–1749; e) X.-L. Yang, M.-H. Xie, C. Zou, Y. He, B. Chen, M. O'Keeffe, C.-D. Wu, *J. Am. Chem. Soc.* **2012**, *134*, 10638–10645.
- [6] a) K. K. Tanabe, S. M. Cohen, *Chem. Soc. Rev.* **2011**, *40*, 498–519; b) Z. Q. Wang, S. M. Cohen, *Chem. Soc. Rev.* **2009**, *38*, 1315–1329.
- [7] T. Yamada, H. Kitagawa, *J Am Chem. Soc* **2009**, *131*, 6312–6313.
- [8] R. Custelcean, M. G. Gorbunova, *J. Am. Chem. Soc.* **2005**, *127*, 16362–16363.
- [9] T. Gadzikwa, O. K. Farha, K. L. Mulfort, J. T. Hupp, S. T. Nguyen, *Chem. Commun.* **2009**, 3720–3722.
- [10] a) J. H. Cavka, S. Jakobsen, U. Olsbye, N. Guillou, C. Lamberti, S. Bordiga, K. P. Lillerud, *J. Am. Chem. Soc.* **2008**, *130*, 13850–13851; b) M. Kandiah, M. H. Nilsen, S. Usseglio, S. Jakobsen, U. Olsbye, M. Tilset, C. Larabi, E. A. Quadrelli, F. Bonino, K. P. Lillerud, *Chem. Mater.* **2010**, *22*, 6632–6640.
- [11] M. Carboni, C. W. Abney, S. Liu, W. Lin, *Chem. Sci.* **2013**, *4*, 2396–2402.
- [12] A. Schaate, P. Roy, A. Godt, J. Lippke, F. Waltz, M. Wiebcke, P. Behrens, *Chem. Eur. J.* **2011**, *17*, 6643–6651.
- [13] a) F. Vermoortele, B. Bueken, G. Le Bars, B. Van de Voorde, M. Vandichel, K. Houthoofd, A. Vimont, M. Daturi, M. Waroquier, V. Van Speybroeck, C. Kirschchock, D. E. De Vos, *J. Am. Chem. Soc.* **2013**, *135*, 11465–11468; b) M. J. Katz, Z. J. Brown, Y. J. Colon, P. W. Siu, K. A. Scheidt, R. Q. Snurr, J. T. Hupp, O. K. Farha, *Chem. Commun.* **2013**, *49*, 9449–9451.
- [14] L. Valenzano, B. Civalleri, S. Chavan, S. Bordiga, M. H. Nilsen, S. Jakobsen, K. P. Lillerud, C. Lamberti, *Chem. Mater.* **2011**, *23*, 1700–1718.
- [15] H. Wu, Y. S. Chua, V. Krungleviciute, M. Tyagi, P. Chen, T. Yildirim, W. Zhou, *J. Am. Chem. Soc.* **2013**, *135*, 10525–10532.
- [16] a) D. W. Feng, Z. Y. Gu, J. R. Li, H. L. Jiang, Z. W. Wei, H. C. Zhou, *Angew. Chem. Int. Ed.* **2012**, *51*, 10307–10310; *Angew. Chem.* **2012**, *124*, 10453–10456; b) W. Morris, B. Voloskiy, S. Demir, F. Gandara, P. L. McGrier, H. Furukawa, D. Cascio, J. F. Stoddart, O. M. Yaghi, *Inorg. Chem.* **2012**, *51*, 6443–6445.
- [17] a) B. Ravel, M. Newville, *J. Synchrotron Radiat.* **2005**, *12*, 537–541; b) J. J. Rehr, R. C. Albers, *Rev. Mod. Phys.* **2000**, *72*, 621–654.
- [18] L. Ma, A. Jin, Z. Xie, W. Lin, *Angew. Chem. Int. Ed.* **2009**, *48*, 9905–9908; *Angew. Chem.* **2009**, *121*, 10089–10092.
- [19] P. L. Llewellyn, G. Maurin, T. Devic, S. Loera-Serna, N. Rosenbach, C. Serre, S. Bourrelly, P. Horcajada, Y. Filinchuk, G. Férey, *J. Am. Chem. Soc.* **2008**, *130*, 12808–12814.
- [20] a) A. Lan, K. Li, H. Wu, D. H. Olson, T. J. Emge, W. Ki, M. Hong, J. Li, *Angew. Chem. Int. Ed.* **2009**, *48*, 2334–2338; b) S. M. Barrett, C. Wang, W. Lin, *J. Mater. Chem.* **2012**, *22*, 10329–10334; c) B. Chen, L. Wang, F. Zapata, G. Qian, E. B. Lobkovsky, *J. Am. Chem. Soc.* **2008**, *130*, 6718–6719.
- [21] a) S. Liu, J. Li, F. Luo, *Inorg. Chem. Commun.* **2010**, *13*, 870–872; b) Y. Xiao, Y. Cui, Q. Zheng, S. Xiang, G. Qian, B. Chen, *Chem. Commun.* **2010**, *46*, 5503–5505; c) Z. Xiang, C. Fang, S. Leng, D. Cao, *J. Mater. Chem. A* **2014**, *2*, 7662–7665; d) Z. Hao, X. Song, M. Zhu, X. Meng, S. Zhao, S. Su, W. Yang, S. Song, H. Zhang, *J. Mater. Chem. A* **2013**, *1*, 11043–11050; e) X.-H. Zhou, L. Li, H.-H. Li, A. Li, T. Yang, W. Huang, *Dalton Trans.* **2013**, *42*, 12403–12409; f) J. Cao, Y. Gao, Y. Wang, C. Du, Z. Liu, *Chem. Commun.* **2013**, *49*, 6897–6899; g) B.-Q. Song, X.-L. Wang, G.-S. Yang, H.-N. Wang, J. Liang, K.-Z. Shao, Z.-M. Su, *CrystEngComm* **2014**, *16*, 6882–6888; h) D. Cai, H. Guo, L. Wen, C. Liu, *CrystEngComm* **2013**, *15*, 6702–6708; i) L. Zhang, Y. Jian, J. Wang, C. He, X. Li, T. Liu, C. Duan, *Dalton Trans.* **2012**, *41*, 10153–10155; j) S. Dang, E. Ma, Z.-M. Sun, H. Zhang, *J. Mater. Chem.* **2012**, *22*, 16920–16926.
- [22] J. K. Taylor, *Quality Assurance of Chemical Measurements*, Lewis Publishers, Boca Raton, FL, **1984**.

 Received: September 6, 2014

Published online on ■■■, 0000

COMMUNICATION

An excellent fluorescence sensor: A metal-organic framework with an orthogonal carboxylic acid moiety adopts a unique eight-connected Zr-oxo secondary building unit, and provides the first direct single-crystal X-ray structure evidence for the proposed “site-defect” phenomenon. Fluorescence of this material is extremely sensitive to the presence of metal cations with unpaired electrons, affording limits of detection below 0.5 ppb and surpassing other MOF sensors by three to four orders of magnitude.



Metal–Organic Frameworks

M. Carboni, Z. Lin, C. W. Abney, T. Zhang,
W. Lin*



A Metal–Organic Framework
Containing Unusual Eight-Connected
Zr–Oxo Secondary Building Units and
Orthogonal Carboxylic Acids for Ultra-
sensitive Metal Detection

